Journal of Applied Physics ARTICLE scitation.org/journal/jap

A quantitative model for the bipolar amplification effect: A new method to determine semiconductor/oxide interface state densities

Cite as: J. Appl. Phys. **130**, 134501 (2021); doi: 10.1063/5.0064397
Submitted: 22 July 2021 · Accepted: 16 September 2021 ·
Published Online: 6 October 2021

James P. Ashton,[1,a)] Stephen J. Moxim,[2] Ashton D. Purcell,[2] Patrick M. Lenahan,[2] and Jason T. Ryan[1]

AFFILIATIONS

[1]Alternative Computing Group, National Institute of Standards and Technology, Gaithersburg, Maryland 20899, USA
[2]Engineering Science and Mechanics Department, The Pennsylvania State University, University Park, Pennsylvania 16802, USA

[a)]**Author to whom correspondence should be addressed:** james.ashton@nist.gov

ABSTRACT

We report on a model for the bipolar amplification effect (BAE), which enables defect density measurements utilizing BAE in metal–oxide–semiconductor field-effect transistors. BAE is an electrically detected magnetic resonance (EDMR) technique, which has recently been utilized for defect identification because of the improved EDMR sensitivity and selectivity to interface defects. In previous work, BAE was utilized exclusively in EDMR measurements. Although BAE EDMR improves the sensitivity of EDMR in studies of semiconductor/oxide interface defects, an understanding of BAE in both electrical measurements and EDMR has not yet been investigated. In this work, we develop a BAE theory based on a modified Fitzgerald–Grove surface recombination methodology, which, in theory, may be utilized to fine-tune conditions for EDMR measurements. BAE may also now be utilized as an analysis tool in purely "electronic" measurements. The model presented here may ultimately prove useful in the development of resonance-based theories of BAE EDMR.

Published by AIP Publishing. https://doi.org/10.1063/5.0064397

I. INTRODUCTION

Understanding spin-dependent transport from a theoretical standpoint dates back to work by Lepine,[1] who investigated spin-dependence of photo-generated carriers on silicon (Si) surfaces. Kaplan, Solomon, and Mott (KSM)[2] further showed that the spin-dependence involves an intermediate state formation between conduction band/valance band carriers and trapped carriers. This new approach was appealing as it explained the large response of spin-dependent recombination (SDR) relative to electron paramagnetic resonance (EPR) (10^7 × improvement)[3] and the field-and-frequency independent response of spin-dependent transport measurements.[2] Refinements have been made to the original work of KSM and Lepine.[4,5] However, recent investigations have introduced the stochastic quantum Liouville equation (SLE) and density matrix formalism to investigate spin-dependent transport.[6–8]

Harmon *et al.* developed a model of spin-dependent recombination (SDR) involving Si/silicon dioxide (SiO_2) interface defects utilizing solutions to the SLE based on the Fitzgerald–Grove surface recombination theory.[9] In this work, they model direct current–current-voltage (dc-IV) SDR experimental measurements, in which the SDR response was modeled as a function of the forward voltage on the source/drain terminals. It is shown that the forward voltage applied to the source/drain terminals alters the rates at which conduction electron and defect electron pairs dissociate or recombine. This is particularly important in near-zero field magnetoresistance (NZFMR),[10,11] where these rates greatly influence the line shape of the NZFMR spectrum.[7,8]

The theoretical framework for the dc-IV method for MOSFET defect density measurements was developed by Fitzgerald and Grove.[9] Reddi *et al.*[12] also utilized a similar theoretical framework to model recombination peaks observed in oxidized bipolar-junction transistors.

In this work, we develop a quantitative treatment of an electrically detected magnetic resonance (EDMR) technique, the bipolar amplification effect (BAE)[13] to measure interface electron–hole recombination at interface defects in MOS devices and present proof-of-concept results on Si MOSFETs. The goal of this work is

to provide a surface recombination model of BAE, which may be utilized as a resource for performing EDMR and purely electronic BAE measurements and for future modeling of the SDR response of BAE EDMR measurements. BAE EDMR is widely utilized as it greatly improves the sensitivity and selectivity of EDMR measurements.[13–19] In systems that have a large contribution from bulk semiconductor defects, such as SiC MOSFETs, dc-IV is ineffective since large contributions from bulk defects would obscure the surface recombination in EDMR measurements. BAE EDMR overcomes the limitations of dc-IV-based EDMR.[13] Therefore, this model may be adapted to solutions of the SLE in the same manner as demonstrated by Harmon *et al.*[7,8] We utilize a modified model based on theory developed by Fitzgerald and Grove[9] and Reddi,[12] in which we account for the variation in carrier distribution throughout the channel region.

A. Direct-current-current–voltage scheme

The dc-IV measurement technique involves the application of a slight forward bias to the source/drain contacts to inject minority carriers into the channel while holding the gate voltage such that the surface is in depletion. A diagram of this biasing scheme is illustrated in Fig. 1. Under the conditions where the surface electron concentration n_s is equal to the surface hole concentration p_s, surface recombination will be maximized. This occurs when[9]

$$n_s = p_s = n_i e^{\frac{qV_F}{2kT}}. \tag{1}$$

Here, $q = 1.602 \times 10^{-19}$ C is electronic charge, V_F is the source/drain-to-body junction forward bias, k is Boltzmann's constant, and T is absolute temperature. Under these conditions, there will be a peak in the recombination current and, subsequently, the body current I_B. According to Fitzgerald and Grove,[9] the amplitude of the current peak can be approximated as

$$\Delta I_B = \frac{2}{\pi} q s_0 n_i \frac{qV_F}{2kT} e^{\frac{qV_F}{2kT}} A_G. \tag{2}$$

Here, A_G is the gate area of the MOSFET and s_0 is the surface recombination velocity given by

$$s_0 \equiv \frac{\pi}{2} \sigma_s v_{th} kT D_{it}. \tag{3}$$

Here, $\sigma_s = \sigma_e = \sigma_h$ is the electron and hole capture cross section, which are assumed to be equivalent. This assumption results in the same expressions for recombination rate as the case when the electron and hole capture cross sections are treated separately.[9] v_{th} is the thermal velocity for both electrons and holes and D_{it} is the density of interface states in $\mathrm{cm}^{-2}\,\mathrm{eV}^{-1}$. Our discussion of the derivation of this expression follows that of Fitzgerald and Grove.[9] We consider an n-channel MOSFET subjected to a gate bias and forward bias applied to the source and drain terminals. Our analysis is for an n-channel device. However, mirror image expressions would also be applicable to p-channel devices. First, we assume that centers have a constant distribution throughout the bandgap. Since recombination is dominated by carriers near midgap, according to Shockley–Read–Hall statistics,[20] this assumption will introduce only modest error, assuming that the density of states does not vary greatly in the near midgap region.[9] The recombination rate per unit area is then given by

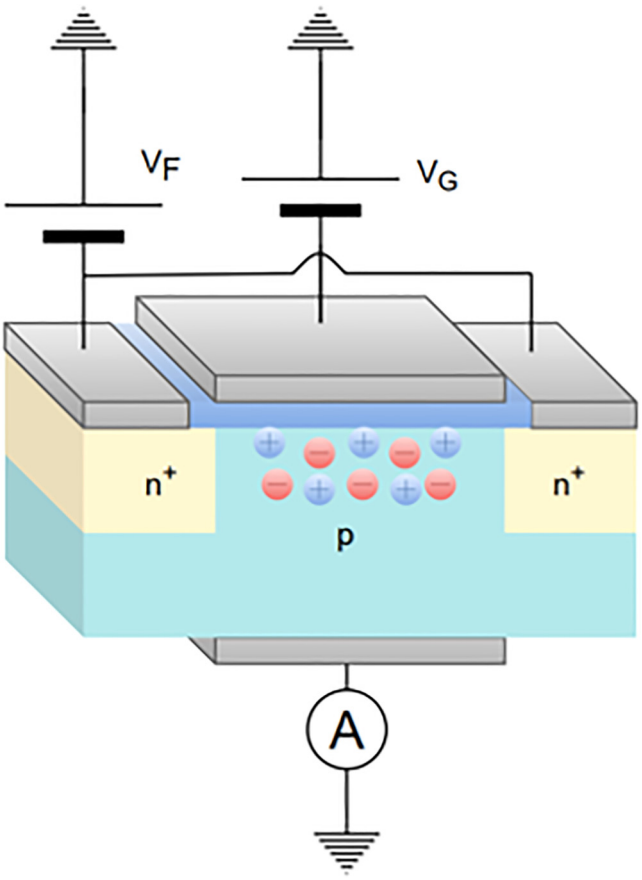

FIG. 1. Illustration of the dc-IV biasing scheme showing the source and drain bias V_F and gate bias V_G.

$$U_S = \sigma_S v_{th} D_{it} \left[\int_{E_v}^{E_c} \frac{dE_{st}}{p_s + n_s + 2n_i \cosh\left(\frac{(E_{st} - E_i)}{kT}\right)} \right] [p_s n_s - n_i^2]. \tag{4}$$

Here, E_v and E_c are the valence and conduction band minimum and maximum, E_{st} is the surface trap energy, and E_i is the intrinsic Fermi energy. Evaluation of (4) leads to the following expression for recombination rate (we only consider the case for $p_s + n_s \geq 2n_i$):[9]

$$U_S = \sigma_S v_{th} kT D_{it} \left[\frac{\cosh^{-1}\left(\frac{p_s + n_s}{2n_i}\right)}{n_i \left[\left(\frac{p_s + n_s}{2n_i}\right)^2 - 1 \right]^{\frac{1}{2}}} \right] [p_s n_s - n_i^2]. \tag{5}$$

If it is further assumed that the condition of quasi-equilibrium is maintained throughout the surface space charge region, the concentration of surface electrons and holes will be functions of the surface potential ϕ_s and V_F,

$$n_s = \frac{n_i^2}{n_A} e^{\frac{q(V_F+\phi_s)}{kT}}, \tag{6a}$$

$$p_s = n_A e^{\frac{-q\phi_s}{kT}}. \tag{6b}$$

Here, n_A is the acceptor doping concentration of the body. By substituting (6) into (5), one may arrive at the model equation for the recombination rate as a function of ϕ_s and V_F. One may relate the surface potential ϕ_s to a gate voltage V_G via[21]

$$V_G = V_{FB} + \phi_s - \frac{Q_S(\phi_s)}{C_{ox}}. \tag{7}$$

Here, V_{FB} is the flatband voltage, $Q_S(\phi_s)$ is the induced semiconductor surface charge, and C_{ox} is the oxide capacitance. What falls out of these substitutions is an expression $U_S = U_S(\phi_s, V_F)$, which may conveniently be considered in three parts. Consider in (5) the first part of the expression on the right, before the fraction, which is characteristic of a velocity involving surface recombination. Next, the fraction represents the effect of surface potential on carrier concentrations. The third part represents the drive of U_S toward equilibrium.[9] This rate will be largest when (1) is satisfied.

Applying (1) to (5)–(7) yields an expression of the form

$$\begin{aligned} U_{Sm} &= \frac{2}{\pi} s_0 n_i \cosh^{-1}\left(e^{\frac{qV_F}{2kT}}\right)\left(e^{\frac{qV_F}{kT}} - 1\right)^{\frac{1}{2}} \\ &\approx \frac{2}{\pi} s_0 n_i \frac{qV_F}{2kT} e^{\frac{qV_F}{2kT}}. \end{aligned} \tag{8}$$

The last approximate equation for U_{Sm} is valid for $V_F \gg kT/q$. Finally, one may arrive at (2) by utilizing

$$\Delta I_B = qA_G U_{Sm}. \tag{9}$$

More generally, the recombination rate $U_S(\phi_s, V_F)$ may be utilized to model the recombination current as a function of gate voltage by utilizing (5)–(7) and

$$I_B = qA_G U_S(V_G, V_F). \tag{10}$$

This equation, plotted with gate voltage, yields a peak in the current, in which the amplitude may be computed via (2) and peak position occurs at precisely $\phi_s = \phi_{fp} - \frac{1}{2}V_F$, where $\phi_{fp} = \frac{kT}{q}\ln\left(\frac{n_A}{n_i}\right)$. This condition is illustrated in Fig. 2. The quantitative BAE method relies on similar principles as those first utilized by Fitzgerald and Grove.[9]

B. Bipolar amplification effect

The BAE[13] scheme is similar to that of dc-IV. However, instead of applying a forward voltage V_F to both source and drain,

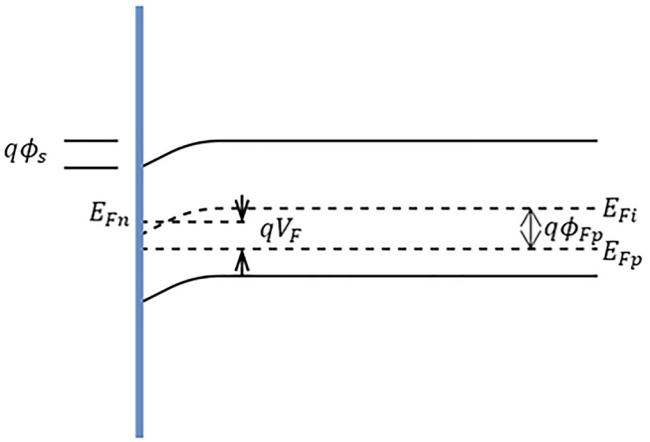

FIG. 2. Surface space charge region under the condition $\phi_s = \phi_{fp} - \frac{1}{2}V_F$, which is the point corresponding to the peak in I_B vs V_G.

the source is disconnected from the drain and the body terminal is grounded. The current is measured through the drain, which is held at virtual ground, and the source bias is held at I_S with a gate bias V_G held in depletion. The source and drain may be flipped here. A diagram of this biasing scheme is illustrated in Fig. 3. This biasing scheme has been extremely effective in EDMR measurements as the sensitivity of the EDMR measurement using BAE is an order of magnitude greater than the dc-IV EDMR approach.[13]

In our discussion of BAE, we consider a constant current bias applied to the source junction I_S instead of the forward bias V_F (V_F is maintained at a value slightly greater than the junction built-in voltage). The drain current, by Kirchoff's law, obeys the following:

$$I_S = I_D + I_B. \tag{11}$$

Here, I_B is the body current (we assume negligible leakage currents through the gate). If we assume that I_S is a constant and $I_B \gg I_D$, then the drain current I_D represents only a small fraction of the total source current I_S. We also assume ohmic contacts for the drain/source and body contacts. Under this approximation, the drain current will consist entirely of electrons and the body will consist entirely of holes since the drain is highly doped (n^+) with ohmic contact for electrons, producing a barrier for holes, and the body is doped p-type with ohmic contact for holes, producing a barrier for electrons. Thus, under EDMR, the change in the drain current ΔI_D is, to a reasonable approximation, equal and opposite to the EDMR-induced change in body current ΔI_B. Since $I_B \gg I_D$, the sensitivity, defined as the relative EDMR change in current $\frac{\Delta I_D}{I_D}$, is orders of magnitude greater at the drain.[13]

Aichinger and Lenahan[13] also note that the EDMR BAE technique is exclusively sensitive to interface defects. Thus, BAE EDMR has been utilized extensively in studies of MOS interface defects.[14–18,22–24] BAE EDMR is quite powerful as the EDMR scheme can be implemented in a wide variety of MOSFET geometries due to the ability to control the range at which minority

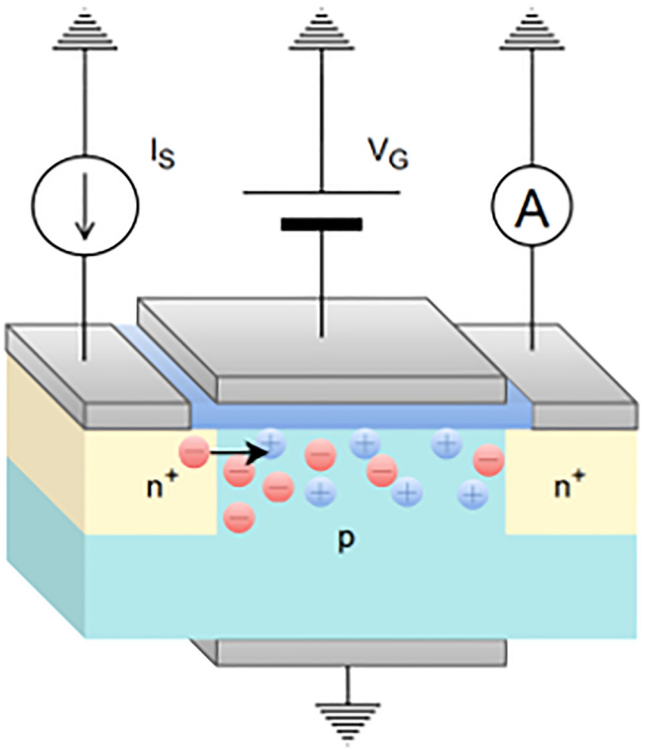

FIG. 3. Illustration of the BAE biasing scheme illustrating a constant current bias I_S on the drain and gate bias V_G.

carriers may diffuse across the channel with a gate voltage V_G. The BAE EDMR scheme is not as limited with regard to channel length, whereas spin-dependent charge pumping (SDCP)[25] is because in BAE EDMR, the gate voltage is utilized to control the length over which minority carriers may travel at the surface. Thus, a small user controlled diffusion current, strongly influenced by surface recombination, may be detected in BAE EDMR.

Two limitations of BAE EDMR are that (1) it cannot provide quantitative information regarding defects and (2) optimal biasing currently relies on trial and error since no predictive models of BAE have been realized. Another weakness is that a model based on BAE EDMR is currently not feasible since spin-dependent recombination and dissociation rates depend upon the forward bias voltage V_F. We hope to address these weaknesses with this model.

C. Electron paramagnetic resonance and electrically detected magnetic resonance

In order to understand some of the results of this paper, a brief discussion of electron paramagnetic resonance (EPR) and EDMR is necessary. The following will briefly discuss the fundamentals of EPR. Consider the simple case of an unpaired electron spin residing at a defect, in which the electron is unperturbed by its local environment. Suppose that a sample with these paramagnetic defects is placed in a microwave cavity and that this cavity is between the pole faces of an electromagnet. The cavity is critically coupled with a microwave source, which generates microwave radiation with photon energy $E = h\nu$, where h is Planck's constant and ν is the microwave frequency. The electromagnet provides a large linearly swept field B_0. The magnetic field splits the energy of the defect electron's $+1/2$ and $-1/2$ spin states. This energy difference is given by $\Delta E = g_e \mu_B B_0$. Here, $g_e \approx 2.0023\ldots''$ is the Landé g factor and μ_B is the Bohr magneton. When the photon energy is equal to the energy difference between the $+1/2$ and $-1/2$ spin states, resonance occurs and the electron's spin "flips." This resonance condition is[26,27]

$$h\nu = g_e \mu_B B_0. \tag{12}$$

Perturbations to the simple case caused by the defect electron's environment provide key information for defect identification. Two of the most important perturbations are spin–orbit coupling and electron–nuclear hyperfine interactions. Spin–orbit coupling alters the Landé g factor g_e into an orientation dependent number g, which is often expressed as a second-rank tensor $\mathbf{g}$. Electron–nuclear hyperfine interactions are caused by nearby magnetic nuclei, which interact with the defect electron and cause additional splitting of the electron energy levels. These interactions can be described via a spin Hamiltonian of the form[26,27]

$$H = \mu_B \mathbf{B} \cdot \mathbf{g} \cdot \mathbf{S} + \sum_i \mathbf{I}_i \cdot \mathbf{A}_i \cdot \mathbf{S}. \tag{13}$$

Here, $\mathbf{B}$ is the applied magnetic field vector, $\mathbf{g}$ is a second rank tensor whose parameters depend upon the spin–orbit coupling interactions, $\mathbf{S}$ is the electron spin angular momentum operator, $\mathbf{I}_i$ is the nuclear spin angular momentum operator for the ith nucleus, and $\mathbf{A}_i$ is the hyperfine coupling tensor for the ith nucleus. Other perturbations exist, such as dipolar and exchange interactions. However, these additional interactions need not be considered in this work.

Conventional EPR has a sensitivity of about 10^{11} defects per mT linewidth.[28] EPR sensitivity is also field and frequency-dependent and the detected response is influenced by every paramagnetic defect within the sample. These limitations are detrimental in studies of micro- and nano-scale electronics devices. EDMR overcomes these limitations. EDMR is about 10^7 times more sensitive than classical EPR[3] and has a sensitivity that is independent of the EDMR field and frequency. An additional advantage of EDMR in nano-and micro-electronic device studies is that EDMR is only sensitive to electrically active defects.

D. Spin-dependent recombination

As previously mentioned, the method of EDMR detection we will be discussing is SDR, which can be can be understood through the seminal work of KSM[2] and subsequent work refining their ideas.[4–6] The following provides a simplified discussion of SDR. Consider a conduction electron that encounters an unpaired electron spin residing at a deep level defect. The conduction electron and trapped electron will couple with form an intermediate spin state. These spin states can either be singlet states ($S = 0$) with basis state $S_0 = (|\uparrow\downarrow\rangle - |\downarrow\uparrow\rangle)/\sqrt{2}$ with $m_S = 0$ or triplet states

($S = 1$) with basis states $T_+ = |\uparrow\uparrow\rangle$, $T_0 = (|\uparrow\downarrow\rangle + |\downarrow\uparrow\rangle)/\sqrt{2}$, and $T_- = |\downarrow\downarrow\rangle$ with $m_S = +1, 0,$ and -1 respectively. For the triplet case, the conduction band to deep level transition will be forbidden by the Pauli exclusion principle, since both electrons will have the same spin quantum number. These triplet states will tend to dissociate and there will be no subsequent electron–hole recombination. However, at resonance, spin flipping events will transform triplet states into singlet states. The resonance-induced singlet state condition renders the transition allowed and permits subsequent electron–hole recombination. In SDR, the flipping of the trap center spins is generally observed.

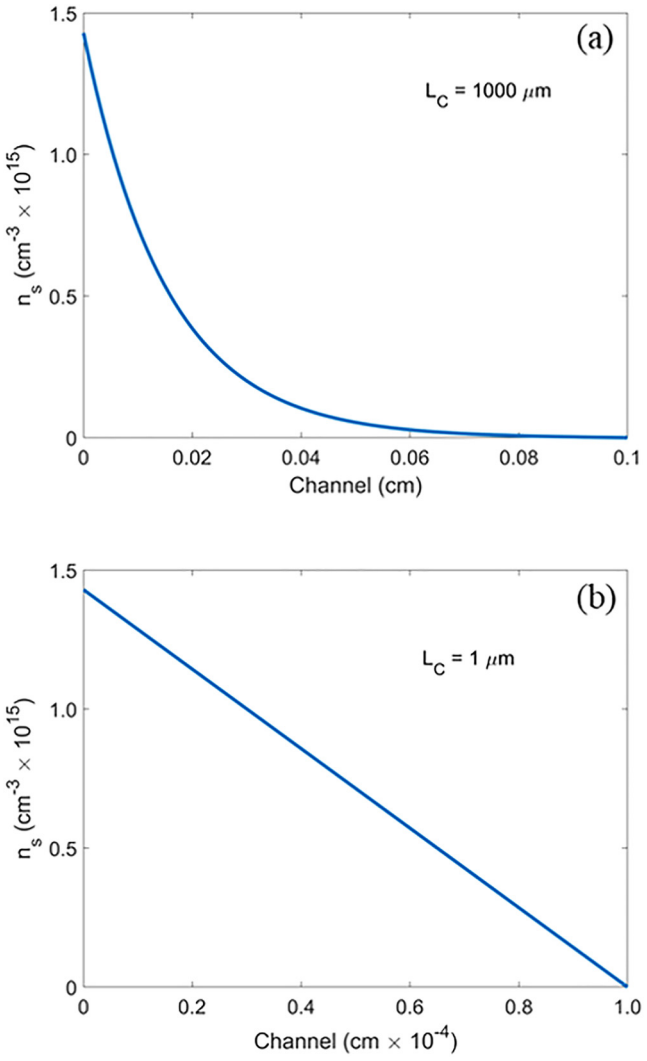

FIG. 4. Distribution of $n_S(x)$ across the channel for a channel length of (a) $L_C = 1000\,\mu$m and (b) $L_C = 1\,\mu$m corresponding to $L_n \ll L_C$ and $L_n \gg L_C$, respectively. In both (a) and (b), a V_F of 0.6 V and a minority carrier lifetime of 30 μs were utilized.[30]

II. MODIFIED FITZGERALD-GROVE MODEL

In our modified model, a forward bias V_F is applied to the source and the current at the drain I_D is monitored. Thus, the drain is at a potential of 0 V, while the source is at a potential of V_F. Therefore, the approximation of quasi-equilibrium throughout the space charge region of (6) must be modified to account for the surface concentrations of electrons and holes along the length of the channel. In order to develop an accurate model for n_s and p_s, we must account for the variation in carrier concentrations along the channel. Assume that the x- direction is along the length of the channel, whose length is defined as L_C.

The MOSFET operation in BAE is similar to that of a gated bipolar-junction transistor in the forward active mode. We begin by writing down the transport equation. Here, we assume that the electron concentration varies only in the x-direction because the high electron concentration layer thickness is negligible compared to L_C. This is a reasonable approximation and is used elsewhere for similar systems,[21,29]

$$D_n \frac{d^2 \delta n_s}{dx^2} - \frac{\delta n_s}{\tau} = 0. \tag{14}$$

Here, D_n is the diffusion coefficient for electrons at the surface, δn_s is the excess surface electron concentration, and τ is the lifetime of electrons. The solution here has the form

$$\delta n_s(x) = Ae^{\frac{x}{L_n}} + Be^{\frac{-x}{L_n}}. \tag{15}$$

Here, L_n is the electron diffusion length, defined as

$$L_n = \sqrt{D\tau}. \tag{16}$$

The values of τ utilized to calculate L_n is 30 μs, which is consistent with lifetime measurements in Si.[30]

The coefficients of (15) can be solved with the boundary conditions

$$\delta n_s(L_C) = n_s(L_C) - n_s = 0, \tag{17a}$$

$$\delta n_s(0) = n_s(0) - n_s = \frac{n_i^2}{n_A} e^{\frac{q\phi_s}{kT}} (e^{\frac{q(V_F)}{kT}} - 1). \tag{17b}$$

The solution to this yields[21]

$$\delta n_s(x) = n_s(e^{\frac{qV_F}{kT}} - 1) \frac{\sinh\left(\frac{L_C - x}{L_n}\right)}{\sinh\left(\frac{L_C}{L_n}\right)}. \tag{18}$$

Thus, the surface electron concentration is $n_s(x) = \delta n_s(x) + n_s$, where $n_s = \frac{n_i^2}{n_A} e^{\frac{q\phi_s}{kT}}$ is the surface concentration far away from the source. With the boundary conditions of (17), (a) is the case at the drain terminal and (b) is the case at the source terminal. We may next utilize (7) to relate ϕ_s to V_G. Note that when $L_C \gg L_n$, $\delta n_s(x)$ can be approximated by $\propto e^{\frac{-x}{L_n}}$. If $L_C \ll L_n$, a linear approximation may be utilized in place of (18). The linear approximation is detailed

elsewhere.[21] A plot of $n_s(x)$ for both extremes, where $L_n \ll L_C$ and $L_n \gg L_C$, is shown in Figs. 4(a) and 4(b), respectively.

In order to account for the varying level of surface recombination across the channel caused by the difference in potential between the source and drain, we may write the surface recombination rate $U_S = U_S(\phi_s, V_F, x)$ utilizing the boundary conditions of (6) modified with spatially dependent surface electron concentration of (18). In order to account for the change in recombination rate over the channel, (10) can be modified by utilization of[31]

$$I_D = qA_G \frac{1}{L_C} \int_0^{L_C} U_S(V_G, V_F, x)dx. \tag{19}$$

We utilize the recombination rate from (5) with modified boundary conditions from (6) and (18) and numerically solve for the drain current utilizing (19).

In Fig. 5, we plot $U_S(\phi_s, x)$ for a simulated $V_F = 0.6$ V. The color bar here represents the magnitude of $U_S(\phi_s, x)$ in units of $cm^{-2}\,s^{-1}$. First note that recombination takes place closer to the source of the device (where V_F is applied) and at low enough band bending such that the average electron and hole carriers are about equal. It should be noted that at 0 along the x-direction (at the source), the rate is maximum at a specific ϕ_s. If one were to multiply this rate by qA_G, one would arrive at the dc-IV peak amplitude. This is so because at position of 0 along x (at the source), the physics is the exact same as that derived by Fitzgerald–Grove.[9] However, in BAE, we must account for the tapering-off of U_S across the channel. A good approximation is that there is an average $U_S(\phi_s, V_F)$ over channel position. Thus, we utilize integration to establish a mean value over the channel length such that we may find a U_S related to only ϕ_s and V_F. ϕ_s may then be related to V_G via (7).

III. EXPERIMENTAL

In our study, we utilized Si MOSFETs with 7.5 nm thick SiO_2 gate oxides. The samples were doped $n_A \approx 5 \times 10^{16}\,cm^{-3}$, in which n_A was extracted from CV measurements. The samples had gate areas $1 \times 15\,\mu m^2$ with 126 transistors chained together. The channel length was $1\,\mu m$. The channel mobility utilized is about $300\,cm^2\,V^{-1}\,s^{-1}$, which was chosen as a limiting case for Si n-channel MOSFETs.[32] The Si MOSFETs were stressed with high field stressing with $V_G = -9.5$ V for 20 min. The stressing created a high density of Si/SiO_2 interface traps.

Our electrical measurements utilized a semiconductor parameter analyzer. The EDMR data was collected utilizing a modified commercial X-band system (9.6 GHz) with an electromagnet and power supply with a temperature-compensated Gaussmeter and Hall probe, a X-band microwave bridge, and a TE_{102} cavity. EDMR device currents were measured with a low-noise current preamplifier. Since EDMR current changes are on the order of pA and our device currents are in the nA range, lock-in detection and magnetic field modulation is utilized. A virtual lock-in amplifier was utilized and magnetic field modulation frequencies in the range of 1 KHz was utilized. Modulation amplitudes were about 0.1 mT.

For the EDMR data, our current measurements have an uncertainty of less than 0.1%, unless otherwise noted. The uncertainty is limited by signal to noise. For the X-band measurements, the uncertainty in g-value calculations is less than 0.0003. The absolute magnetic field was calibrated with a "strong pitch" spin standard. For the Si EDMR data, a backward and forward moving average filter was utilized. The signal to noise before filtering was about 40:1. The uncertainty in peak heights of the electrical curves is no greater than 3%.

IV. RESULTS

Figure 6 shows IDVD measurements from the Si MOSFETs. It should be noted again that these samples were stressed with high

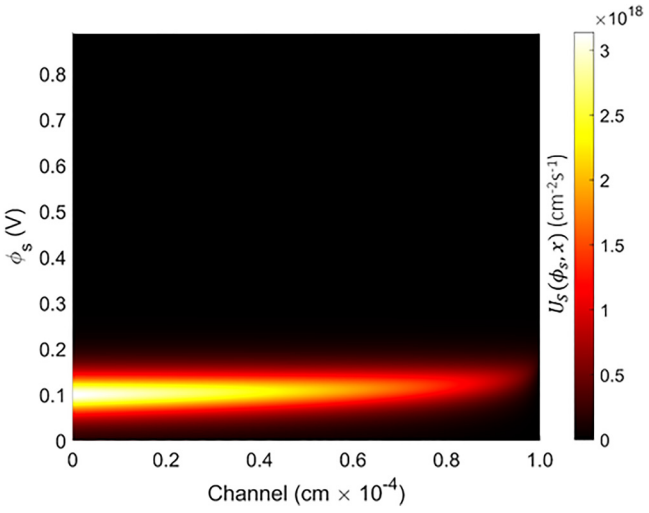

FIG. 5. Simulated BAE $U_S(\phi_s, x)$ with $V_F = 0.6$ V.

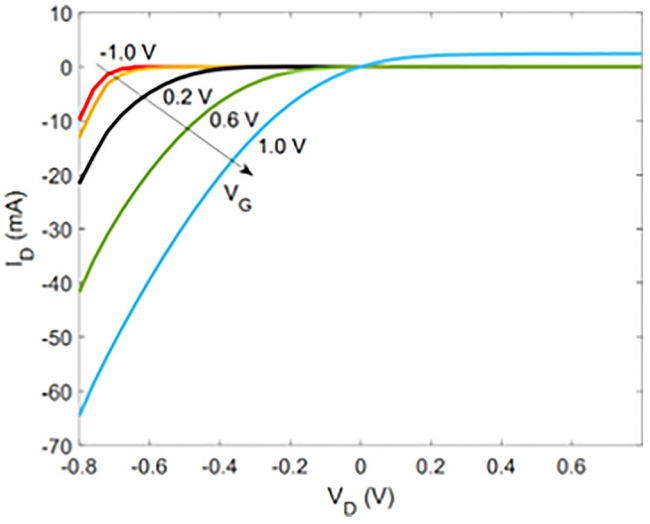

FIG. 6. IDVD measurements on the Si MOSFETs.

field stressing, which is discussed in the Experimental section. The stressing induces a high density of Si/SiO_2 interface defects.

In order to confirm defect density counts in the Si MOSFETs, charge pumping (CP)[33–35] measurements have been performed (not shown). We extract a defect density of $1.9 \times 10^{12}\ cm^{-2}\ eV^{-1}$. The range of the bandgap explored with our charge pumping measurements is about 49%. This percentage is in agreement with the literature for charge pumping measurements in Si MOS at room temperature.[36]

We also performed dc-IV measurements on the Si MOSFETs. The results are shown in Fig. 7. Here, the source/drain-to-body junctions were forward biased at $V_F =$ to 0.48 V. We assumed a capture cross section of $4 \times 10^{-16}\ cm^2$.[37] From the peak of the dc-IV curve, utilizing (2), we extract a defect density of $1.7 \times 10^{12}\ cm^{-2}\ eV^{-1}$.

We performed BAE electrical measurements by forward biasing the source junction and measuring current at the source/drain. We utilize $V_F = 0.48$ to 0.60 V in increments of 0.04 V. The results are shown in Fig. 8. Here, the solid lines represent the experimental BAE current, extracted from the difference between the magnitude of the source and drain current (this was required because the drain current rises steeply as threshold voltage is approached). The dashed line shows the model BAE current calculated from (19). Note the close correspondence between experimental and theory curve peaks and positions. As Fitzgerald and Grove explains in their original surface recombination theory, the difference in peak width can be explained by microscopic nonuniformities of the surface potential caused by a random distribution of surface charges.[9] From the fit of the theory curves, a defect density of $1 \times 10^{12}\ cm^{-2}\ eV^{-1}$ was extracted. It should be noted that a window of $\approx \frac{1}{2} qV_F$ of the middle of the bandgap is explored with both dc-IV and BAE.

We next compare the original Fitzgerald–Grove model to the modified model taking into account different quasi- Fermi levels on each side of the channel, resulting in a gradient of electron concentration across the channel. The results are plotted in Fig. 9.

It is clear from this plot that the modified model peaks are smaller than those predicted by Fitzgerald–Grove. This is because of the difference in quasi-Fermi levels at the source and drain. Assuming a linear carrier distribution along the channel (for $L_n \gg L_C$), which is usually the case for *Si* MOSFETs, and assuming $qV_F \gg kT$, a good approximation for the peak amplitude of the BAE is given by

$$\Delta I_{BAE} \approx \frac{2}{3}\left[\frac{1}{2} q\sigma_s v_{th} D_{it} n_i A_G q V_F \left(e^{\frac{qV_F}{2kT}}\right)\right] = \frac{2}{3}\Delta I_B. \tag{20}$$

Here, ΔI_B is the same as in (2) and is the body current measured during dc-IV utilizing the same biasing conditions. Through numerical integration of the simulated BAE peaks and comparing amplitudes to simulated dc-IV peak amplitudes, one arrives at a ratio of ≈0.62, which is fairly consistent with V_F. Thus, the BAE peaks are $\approx \frac{2}{3}$ the size of the dc-IV peaks at the same conditions. Again, this is assuming that $qV_F \gg kT$ and, again, $L_n \gg L_C$. If the surface electron concentration gradient is not quite linear, the actual ratio will be smaller than $\frac{2}{3}$. Thus, $\frac{2}{3}$ is an approximate upper limit to $\frac{\Delta I_{BAE}}{\Delta I_B}$.

Thus, the peak amplitudes depend upon the free carrier concentration gradient at the interface and this gradient alters both the effect of the surface potential on carrier concentrations and on the driving force toward equilibrium. It should be noted that in reference to Fig. 2, the point at which electron and hole densities are equal (1) in BAE is $\phi_s \approx \phi_{fp} - \frac{1}{2} V_F$, approximately the same as dc-IV.

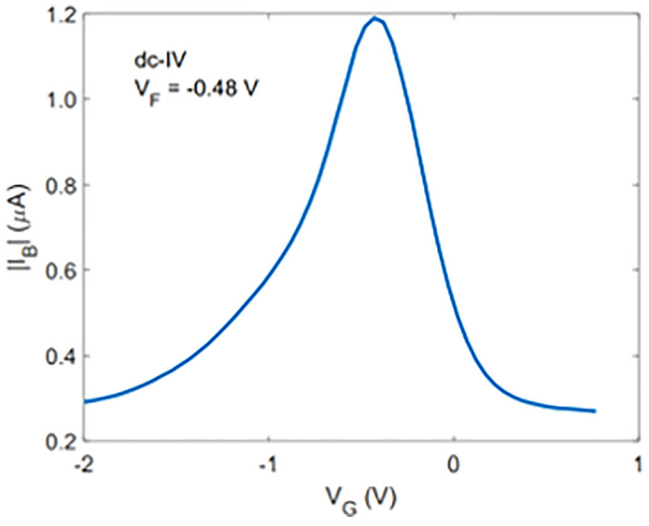

FIG. 7. dc-IV measurements on the Si MOSFETs. Here, $V_F = V_{S/D} = 0.48$ V.

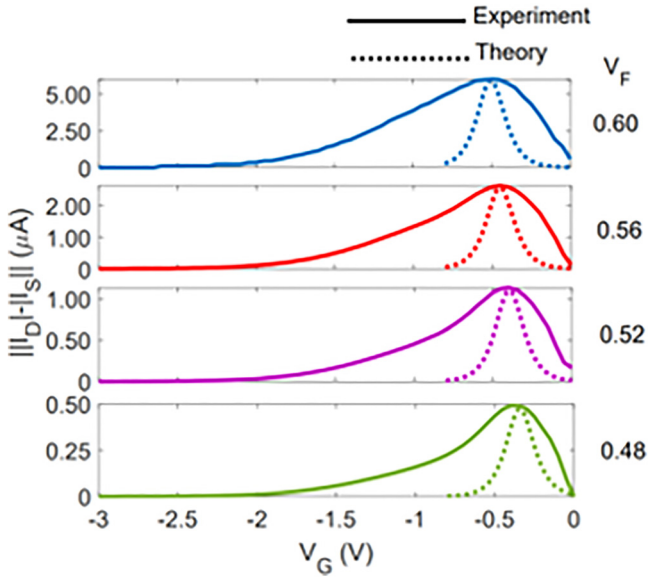

FIG. 8. BAE measurements on the Si MOSFETs. The source voltage V_F was stepped from 0.48 V to 0.60 V in 0.04 V increments.

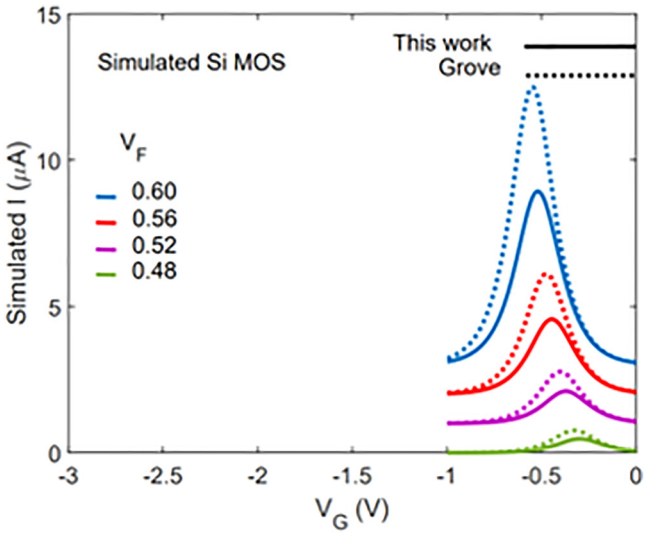

FIG. 9. Comparison of the Fitzgerald–Grove[9] model and the modified model of this work for Si. The simulated source voltage V_F was stepped from 0.48 V to 0.60 V in 0.04 V increments.

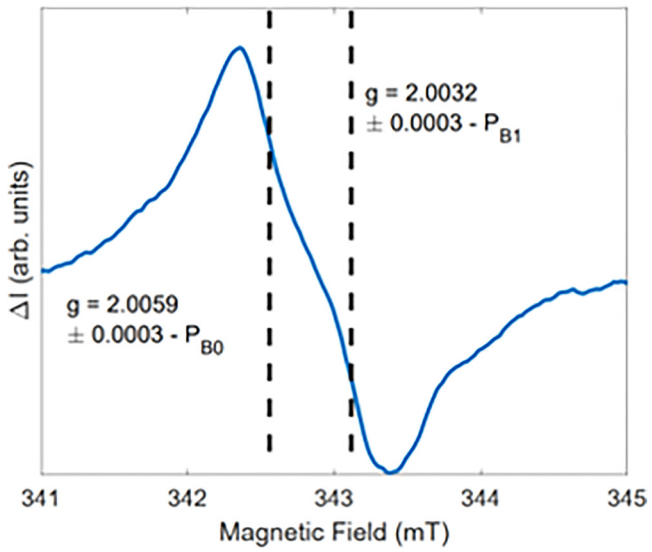

FIG. 11. Representative BAE EDMR spectrum of the Si MOSFET. The spectrum consists of two overlapping lines. Note the $g = 2.0060 \pm 0.0003$ and 2.0030 ± 0.0003, consistent with P_{B0} and P_{B1} centers, respectively.

For the case of Si, this is observed in comparing the two schemes at the same forward bias V_F, as shown in Fig. 10. Note the close correspondence between the *trend* of the data with bias between Figs. 9 and 10. A similar trend is observed for even larger biases. The dc-IV peaks are larger than $\frac{3}{2}$ the BAE peaks. The actual measured ratios are consistently between 0.5 to 0.6. Again, the discrepancy between the theoretically predicted ratios and experimentally observed is within the limits of our approximations. If the interface surface electron gradient strays from linear, the form of (18) would have to be utilized for the surface electron concentration and the actual ratio would be smaller than $\frac{2}{3}$.

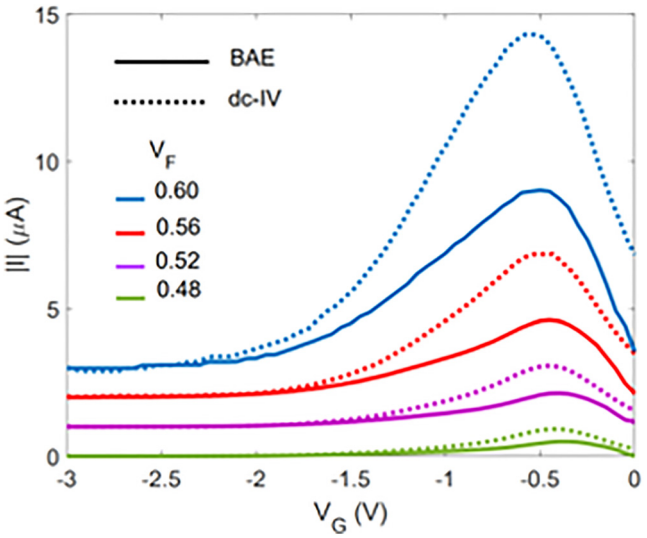

FIG. 10. Comparison of BAE and dc-IV measurements on the Si MOSFET. The source voltage (BAE) and source/drain voltage (dc-IV) (V_F) was stepped from 0.48 V to 0.60 V in 0.4 V increments.

In addition, as noted by Aichinger and Lenahan,[13] BAE EDMR measurements are highly sensitive and highly selective to only the most important defects in MOS technology, namely, the semiconductor/oxide interface. In Fig. 11, we plot the BAE EDMR spectrum of the Si MOSFET. Here, the g values measured are consistent with silicon dangling bonds known as P_{b0} and P_{b1} centers.[38,39]

Thus, we have shown, as a proof-of-concept, that in the Si/SiO_2 system, BAE can now be utilized as a quantitative tool to extract defect densities and provide defect structure.

V. DISCUSSION AND CONCLUSIONS

A model has been developed for the BAE technique, in which proof-of-concept results are demonstrated on Si/SiO_2 MOSFETs. Much like dc-IV, the densities of defects may be extracted from utilization of theory developed by Fiztgerald and Grove.[9] However, integration of a spatially dependent recombination rate (19) extends the original Fitzgerald–Grove model to account for the difference in the quasi-Fermi levels at the source and drain.

The presented model accurately predicts the peaks for Si and differences between dc-IV and BAE peak intensities are also accounted for utilizing the modified model presented here. The extracted defect densities for Si are reasonable. The Si D_{it} values are quite high in comparison with the literature.[38] The high density of defects in the Si devices is the result of high field stressing. The CP measurements in Si measures about 49% of the bandgap and the

BAE and dc-IV schemes measure $\approx \frac{1}{2} q V_F$. The defect densities measured by all three schemes (dcIV, BAE, and CP) are reasonably consistent with one another.

Since the modified model presented here depends upon differences in potential from the source and drain of the MOSFET, the modified model may be utilized to develop a relatively accurate BAE EDMR/NZFMR model utilizing solutions to the SLE. The modified model should explain differences in BAE EDMR/NZFMR and dc-IV EDMR/NZFMR through predictions of differences in singlet/triplet dissociation rates observed in comparing the two measurement schemes. However, this is the subject of future experimental and modeling investigations.

Another potential utility of the quantitative BAE method is that it may also be utilized for estimating carrier lifetimes by performing both BAE and dc-IV in devices with varying channel lengths. This is because when the surface carrier concentration is linear ($L_n \gg L_C$), the ratio of the BAE peak intensity to dc-IV peak intensity $\frac{\Delta I_{BAE}}{\Delta I_B}$ is constant ($\approx \frac{2}{3}$) across channel lengths well below L_n. However, when L_C approaches L_n, the ratio $\frac{\Delta I_{BAE}}{\Delta I_B}$ begins to drop below $\frac{2}{3}$. At the point where this occurs, L_n may be estimated.

We present a simple quantitative model for BAE, which may now be utilized to determine defect densities within the midgap range in MOSFETs. The quantitative BAE measurement is demonstrated in a proof-of-concept on Si MOS devices. The densities extracted are compared against more traditional schemes, such as CP and dc-IV. We find a close agreement between CP, dc-IV, and quantitative BAE. The model presented here thus extends BAE from an EDMR measurement, which is utilized to study defect structure, to a quantitative measurement. In addition, the model may potentially be utilized in BAE EDMR measurements to optimize biasing in order to maximize the SDR in MOS devices. Future work will consist of (1) developing models for BAE EDMR, in which the results from this work will be utilized in conjunction with solutions to the SLE, which have already proven useful in models of dc-IV SDR,[7,8] and (2) performing BAE and dc-IV measurements in devices with varying channel lengths to determine L_n.

ACKNOWLEDGMENTS

The authors would like to thank Fedor Sharov for assistance in technical discussions and sample work and David R. Hughart and Gaddi S. Haase of Sandia National Laboratories for providing the samples utilized in this work. This project was sponsored by the Department of Defense, Defense Threat Reduction Agency under Grant No. HDTRA1-18-0012. The content of the information does not necessarily reflect the position or the policy of the federal government, and no official endorsement should be inferred.

AUTHOR DECLARATIONS

Conflict of Interest

The authors have no conflicts to disclose.

DATA AVAILABILITY

The data that support the findings of this study are available from the corresponding author upon reasonable request.

REFERENCES

[1]D. J. Lepine, "Spin-dependent recombination on silicon surface," Phys. Rev. B **6**, 436–441 (1972).
[2]D. Kaplan, I. Solomon, and N. Mott, "Explanation of the large spin-dependent recombination effect in semiconductors," J. Phys. Lett. **39**, 51–54 (1978).
[3]M. Stutzmann, M. S. Brandt, and M. W. Bayerl, "Spin-dependent processes in amorphous and microcrystalline silicon: A survey," J. Non-Cryst. Solids **266–269**, 1–22 (2000).
[4]F. C. Rong, W. R. Buchwald, E. H. Poindexter, W. L. Warren, and D. J. Keeble, "Spin-dependent Shockley-Read recombination of electrons and holes in indirect-band-gap semiconductor p-n junction diodes," Solid State Electron. **34**, 835–841 (1991).
[5]C. Boehme and K. Lips, "Theory of time-domain measurement of spin-dependent recombination with pulsed electrically detected magnetic resonance," Phys. Rev. B **68**, 245105 (2003).
[6]R. Haberkorn and W. Dietz, "Theory of spin-dependent recombination in semiconductors," Solid State Commun. **35**, 505–508 (1980).
[7]N. J. Harmon, S. R. Mcmillan, J. P. Ashton, P. M. Lenahan, and M. E. Flatté, "Modeling of near zero-field magnetoresistance and electrically detected magnetic resonance in irradiated Si/SiO_2 MOSFETs," IEEE Trans. Nucl. Sci. **67**, 1669–1673 (2020).
[8]N. J. Harmon, J. P. Ashton, P. M. Lenahan, and M. E. Flatté, "Near-zero-field spin-dependent recombination current and electrically detected magnetic resonance from the Si/SiO_2 interface," arXiv:2008.08121 [cond-mat.mtrl-sci] (2020).
[9]D. Fitzgerald and A. Grove, "Surface recombination in semiconductors," Surf. Sci. **9**, 347–369 (1968).
[10]C. J. Cochrane and P. M. Lenahan, "Zero-field detection of spin dependent recombination with direct observation of electron nuclear hyperfine interactions in the absence of an oscillating electromagnetic field," J. Appl. Phys. **112**, 123714 (2012).
[11]J. P. Ashton, S. J. Moxim, P. M. Lenahan, C. G. Mckay, R. J. Waskiewicz, K. J. Myers, M. E. Flatté, N. J. Harmon, and C. D. Young, "A new analytical tool for the study of radiation effects in 3-D integrated circuits: Near-zero field magnetoresistance spectroscopy," IEEE Trans. Nucl. Sci. **66**, 428–436 (2019).
[12]V. Reddi, "Influence of surface conditions on silicon planar transistor current gain," Solid State Electron. **10**, 305–334 (1967).
[13]T. Aichinger and P. M. Lenahan, "Giant amplification of spin dependent recombination at heterojunctions through a gate controlled bipolar effect," Appl. Phys. Lett. **101**, 083504 (2012).
[14]T. Umeda, Y. Kagoyama, K. Tomita, Y. Abe, M. Sometani, M. Okamoto, S. Harada, and T. Hatakeyama, "Electrically detected-magnetic-resonance identifications of defects at 4H-SiC(000$\bar{1}$)/SiO_2 interfaces with wet oxidation," Appl. Phys. Lett. **115**, 151602 (2019).
[15]T. Umeda, T. Kobayashi, M. Sometani, H. Yano, Y. Matsushita, and S. Harada, "Carbon dangling-bond center (carbon P_b center) at 4H-SiC(0001)/SiO_2 interface," Appl. Phys. Lett. **116**, 071604 (2020).
[16]T. Umeda, Y. Nakano, E. Higa, T. Okuda, T. Kimoto, T. Hosoi, H. Watanabe, M. Sometani, and S. Harada, "Electron-spin-resonance and electrically detected-magnetic-resonance characterization on P_bC center in various 4H-SiC (0001)/SiO_2 interfaces," J. Appl. Phys. **127**, 145301 (2020).
[17]J. P. Ashton, P. M. Lenahan, D. J. Lichtenwalner, A. J. Lelis, and M. A. Anders, "Electrically detected magnetic resonance study of barium and nitric oxide treatments of 4H-SiC metal-oxide-semiconductor field-effect transistors," J. Appl. Phys. **126**, 145702 (2019).
[18]J. Cottom, G. Gruber, G. Pobegen, T. Aichinger, and A. L. Shluger, "Recombination defects at the 4H-SiC/SiO_2 interface investigated with electrically detected magnetic resonance and *ab initio* calculations," J. Appl. Phys. **124**, 045302 (2018).
[19]G. Gruber, J. Cottom, R. Meszaros, M. Koch, G. Pobegen, T. Aichinger, D. Peters, and P. Hadley, "Electrically detected magnetic resonance of carbon dangling bonds at the Si-face 4H-SiC/SiO_2 interface," J. Appl. Phys. **123**, 161514 (2018).

[20]W. Shockley and W. T. Read, "Statistics of the recombination of holes and electrons," Phys. Rev. **87**, 835–842 (1952).
[21]Y. Taur and T. Ning, *Fundamentals of Modern VLSI Devices* (Cambridge University Press, 2013).
[22]C. J. Cochrane, P. M. Lenahan, and A. J. Lelis, "The effect of nitric oxide anneals on silicon vacancies at and very near the interface of 4H-SiC metal oxide semiconducting field effect transistors using electrically detected magnetic resonance," Appl. Phys. Lett. **102**, 193507 (2013).
[23]R. J. Waskiewicz, M. A. Anders, P. M. Lenahan, and A. J. Lelis, "Ionizing radiation effects in 4H-SiC nMOSFETs studied with electrically detected magnetic resonance," IEEE Trans. Nucl. Sci. **64**, 197–203 (2017).
[24]J. P. Ashton, P. M. Lenahan, D. J. Lichtenwalner, and A. J. Lelis, "Leakage currents and E' centers in 4H-SiC MOSFETs with barium passivation," in *2020 IEEE International Reliability Physics Symposium (IRPS)* (IEEE, 2020), pp. 1–4.
[25]B. C. Bittel, P. M. Lenahan, J. T. Ryan, J. Fronheiser, and A. J. Lelis, "Spin dependent charge pumping in SiC metal-oxide-semiconductor field-effect-transistors," Appl. Phys. Lett. **99**, 083504 (2011).
[26]W. Gordy, *Theory and Applications of Electron Spin Resonance* (John Wiley & Sons, New York, 1980).
[27]C. Slichter, *Principles of Magnetic Resonance*, 3rd ed. (Springer-Verlag, Berlin, 1978).
[28]G. R. Eaton, S. S. Eaton, D. P. Barr, and R. T. Weber, *Quantitative EPR* (Springer, New York, 2010).
[29]K. Sheng, S. Finney, and B. Williams, "A new analytical IGBT model with improved electrical characteristics," IEEE Trans. Power Electron. **14**, 98–107 (1999).
[30]D. K. Schroder, "Carrier lifetimes in silicon," IEEE Trans. Electron Devices **44**, 160–170 (1997).
[31]A. Grove, *Physics and Technology of Semiconductor Devices* (John Wiley & Sons, Berkeley, 1967), p. 366.
[32]E. Sangiorgi and M. R. Pinto, "A semi-empirical model of surface scattering for Monte Carlo simulation of silicon n-MOSFETs," IEEE Trans. Electron Devices **39**, 356–361 (1992).
[33]G. Groeseneken, H. E. Maes, N. Beltran, and R. F. D. E. Keersmaecker, "A reliable approach to charge-pumping measurements in MOS transistors," IEEE Trans. Electron Devices **ED-31**, 42–53 (1984).
[34]A. B. Elliot, "The use of charge pumping currents to measure surface state densities in MOS transistors," Solid State Electron. **19**, 241–247 (1976).
[35]S. J. Brugler and P. G. Jespers, "Charge pumping in MOS devices," IEEE Trans. Electron Devices **ED-16**, 297–302 (1969).
[36]M. Hori and Y. Ono, "Charge pumping under spin resonance in Si(100) metal-oxide-semiconductor transistors," Phys. Rev. Appl. **11**, 064064 (2019).
[37]J. T. Ryan, A. Matsuda, J. P. Campbell, and K. P. Cheung, "Interface-state capture cross section—Why does it vary so much?," Appl. Phys. Lett. **106**, 163503 (2015).
[38]M. A. Jupina and P. M. Lenahan, "Spin dependent recombination: A ^{29}Si hyperfine study of radiation-induced P_B centers at the Si/SiO_2 interface," IEEE Trans. Nucl. Sci. **37**, 1650–1657 (1990).
[39]P. M. Lenahan and M. A. Jupina, "Spin dependent recombination at the silicon/silicon dioxide interface," Colloids Surf. **45**, 191–211 (1990).